Insights into the Signal Transduction Mechanism of *Rm*FixL Provided by Carbon Monoxide Recombination Kinetics†

Kenton R. Rodgers,*,‡ Lei Tang,‡ Gudrun S. Lukat-Rodgers,‡ and Nancy L. Wengenack§

Department of Chemistry, North Dakota State University, Fargo, North Dakota 58105, and Department of Biochemistry and Molecular Biology, Mayo Clinic and Foundation, Rochester, Minnesota 55905

Received June 15, 2001; Revised Manuscript Received August 14, 2001

ABSTRACT: This report presents evidence for interdomain steps of the ligand-coupled signal transduction mechanism of the oxygen receptor from *Rhizobium meliloti*, *Rm*FixL. Photolysis of the CO adducts of heme domain (*Rm*FixLN) and heme kinase (*Rm*FixL*) proteins allowed tracking of second-order heme CO recombination reactions by transient absorbance. Whereas CO rebinding to *Rm*FixLN is characterized by a single kinetic phase, rebinding to *Rm*FixL* is characterized by two kinetic phases. Evidence indicates that CO rebinds to two interconvertible deoxy*Rm*FixL* conformers that are produced sequentially after photolysis. Since the second conformer is only observed when the kinase domain is present, its production is concluded to be an interdomain signal transmission event that is coupled to heme ligand release. Because receptor clustering is a recurring theme in signal transduction mechanisms, the dependence of molecular weight upon heme ligation was investigated at equilibrium. Gel permeation chromatography and native gel electrophoresis showed that the molecular weight distribution for both *Rm*FixLN and *Rm*FixL* depends on heme ligation. At equilibrium, oxy*Rm*FixLN and oxy*Rm*FixL* exist as monomers and dimers, respectively. Their deoxy analogues, met*Rm*FixLN and met*Rm*FixL*, exist as dimers and as a mixture of tetramers and 9-mers, respectively. Assembly of these oligomers is reversible. The physiological relevance of these ligand-coupled assemblies and the kinetic factors controlling CO recombination are discussed.

The O_2 sensor, *Rhizobium meliloti* FixL (*Rm*FixL),[1] regulates the genes required for N_2 fixation (*1*). It consists of a transmembrane domain, a heme-containing PAS domain, and a histidine kinase domain (*2, 3*). Binding and release of O_2 by the ferrous heme are communicated to the kinase domain and control its autophosphorylation activity with ATP. *Rm*FixL then regulates activity of the transcriptional activator, FixJ, via phosphoryl transfer (*4, 5*). Deoxy*Rm*FixL (ferrous heme) and other high-spin (HS) forms such as met*Rm*FixL (ferric heme) exhibit kinase activity. The kinase activity of oxy*Rm*FixL (ferrous O_2 bound) and other low-spin (LS) six-coordinate (6-c) heme adducts is inhibited (*6*). Initially, a spin state model in which kinase activity is responsive to the spin state of the heme was proposed (*6*). Subsequent studies have pointed to the exogenous ligand occupancy of the distal heme pocket as an important factor in communication between the heme and kinase domains (*7*−*9*). More detailed insights into the mechanism of signal transmission have only recently been gained (*10*−*13*).

Several mechanistic models have been proposed for communication of O_2 uptake by the heme, which sits with a cavity between the α-helix and β-sheet structures of the PAS fold (*10, 12*), to the kinase domain. On the basis of comparison of the crystal structures of five-coordinate (5-c) HS ferric, 6-c LS ferric cyanide, and 6-c LS oxy forms of the heme domain of *Bradyrhizobium japonicum* FixL (*Bj*FixL), it has been suggested that the allosteric mechanism of FixL is unique and relies on rearrangement of H-bonding between heme 6,7-propionates and the FG loop in response to heme doming/flattening upon ligand dissociation/association (*10, 12*). *Bj*FixL is 50% homologous with *Rm*FixL (*14*).

A second model involving steric interactions on the distal side of the heme when O_2 binds has been proposed (*7, 9, 13, 15*). Resonance Raman and UV−visible spectroscopic characterization and autophosphorylation activity of *Rm*FixL mutated at Ile209 and Ile210 indicate that these residues are important in communication between the heme and kinase domains. Conformational changes in the highly flexible Ile209 and Ile210 residues upon O_2 binding heme and steric interactions of their side chains with bound O_2 are proposed to be the first step in signal transduction to the kinase domain (*13, 15*).

Finally, a model of interdomain signaling which involves propagation of ligation-coupled conformational motion originating from both sides of the heme has been proposed (*16*). Reports of resonance Raman studies of the CO and NO adducts of *Rm*FixL* and *Rm*FixLN have revealed different distal pocket conformations in the two proteins (*7, 16*−*18*). These data support the conclusion that the kinase domain

† This work was supported by U.S. Department of Agriculture Grant 97-35305-5158 (K.R.R.) and Hermann Frasch Foundation Grant 446-HF97 (K.R.R.).

* To whom correspondence should be addressed. Telephone: (701) 231-8746. Fax: (701) 231-8831. E-mail: kent_rodgers@ndsu.nodak.edu.

‡ North Dakota State University.

§ Mayo Clinic and Foundation.

[1] Abbreviations: 6-c, six-coordinate; 5-c, five-coordinate; LS, low-spin; HS, high-spin; *Rm*FixL, *R. meliloti* FixL; *Rm*FixL*, soluble truncated *Rm*FixL containing heme and kinase domains; *Rm*FixLN, heme domain of *Rm*FixL; *Bj*FixL, *B. japonicum* FixL; HbA, hemoglobin A; TA, transient absorbance; EXAFS, extended X-ray absorption fine structure; TC, thermocouple.

10.1021/bi011237q CCC: $20.00
Published on Web 10/04/2001

constrains the distal heme pocket and the Fe−C−O and Fe−N−O conformations. This points to involvement of distal interaction in interdomain signal transduction and is consistent with the distal mutations that disrupt interdomain communication (*13*, *15*). In addition, nanosecond time-resolved rR spectra show transient compression of the Fe−His bond after CO photolysis, but before formation of equilibrium deoxy*Rm*FixL wherein the kinase is active (*11*). A direct correlation between the kinase activity and the distance between the mean heme plane and the proximal imidazole was revealed by EXAFS studies of five *Rm*FixL ligand complexes (*17*). These data support involvement of the proximal side of the heme in communicating the heme ligation state.

Examining the rates of CO coordination to the heme of *Rm*FixL provides a view into the signal transduction between the heme and kinase domains. Like O_2 binding, CO binding inhibits kinase activity of *Rm*FixL (*6*). The photolabile nature of the Fe−CO bond in the *Rm*FixL−CO adduct allows for laser-induced dissociation of the CO. This property is particularly useful as a rapid trigger in initiating conversion of kinase-inactive (CO-bound) to kinase-active (5-c HS ferrous) *Rm*FixL. This photolysis enables kinetic studies probing the dynamics of the active site. In this study, the kinetic behavior of CO recombination is examined for two soluble derivatives of *Rm*FixL, *Rm*FixLN and *Rm*FixL*. *Rm*FixLN, the heme domain of *Rm*FixL, binds oxygen but lacks kinase activity (*2*). *Rm*FixL* contains the heme domain and the C-terminal kinase domain of *Rm*FixL; it binds oxygen, exhibits kinase activity, and transfers its phosphate group to *Rm*FixJ (*4*). The bimolecular CO recombination kinetics of *Rm*FixLN reveal a single kinetic phase. However, two kinetic phases are observed for bimolecular *Rm*FixL*−CO recombination. These results are consistent with a conformational transition that (a) involves the kinase domain and (b) is coupled to release of the heme ligand. The relevance of the second phase to the mechanism of signal transduction is discussed.

MATERIALS AND METHODS

Protein Preparation. *Rm*FixLN and *Rm*FixL* were obtained as previously described (*2*, *7*). They were purified to homogeneity, as judged by SDS−PAGE. The proteins were fully loaded with heme based on the purity indices, R_z (A_{397}/A_{280}), for ferric *Rm*FixL* and *Rm*FixLN of 2.8 and 4.0, respectively. Autophosphorylation activity of *Rm*FixL* was measured by ^{32}P tracer methods using [γ-^{32}P]ATP (*2*, *7*). Activities were in line with published values (*2*, *7*, *15*). Interconversions of the ferric, ferrous, and ferrous carbonyl forms of both proteins were confirmed by UV−visible spectroscopy. UV−visible spectra were recorded on a scanning double spectrometer under microcomputer control. The spectrometer was calibrated against the holmium oxide glass spectrum.

Preparation of FixL−CO Adducts. Deoxy forms of *Rm*FixL* and *Rm*FixLN (15−100 μM in heme) were generated anaerobically in an ice bath by treatment of ferric *Rm*FixL* and *Rm*FixLN with approximately 2 redox equiv of a buffered sodium dithionite solution. The corresponding CO adducts were prepared by flushing the ferrous proteins with CO or a mixture of CO and N_2 with the CO:N_2 molar ratio controlled by calibrated flow meters. The solubility of CO in the protein solution was taken to be the same as that in water and was calculated using Henry's Law. The concentration of CO in solution was calculated from the partial pressure of CO over the solution, which was corrected for the vapor pressure of water. Protein samples were in 20 mM Tris-HCl buffer (pH 7.8) and 100 mM NaCl. Samples were loaded anaerobically into quartz ESR flat cells having an optical path length of 0.36 mm.

Measurement of CO Recombination Rates. All rate measurements were carried out under psuedo-first-order conditions with CO in large excess. The CO ligand was photodissociated with a 3 ns, 532 nm laser flash from an injection-seeded Nd:YAG laser having a "top hat" beam profile. The pulse repetition rate of the Nd:YAG laser was 0.5 Hz (unless otherwise noted) to ensure the system had returned to equilibrium prior to the next pulse. For single-wavelength measurements, a low-intensity beam from a wavelength-filtered quartz halogen lamp was used to track absorbance during CO recombination. The photolysis and probe beams were overlapped such that the pump beam diameter was approximately 1.5 times that of the probe. Light transmitted through the sample was focused on the slit of a 0.3 m monochromator equipped with a 1800 groove/mm grating and a photomultiplier tube. The PMT output was recorded with a digital sampling oscilloscope. Digital sampling rates ranged from 0.5 to 10 kHz. Absorbance was monitored at 440 nm during CO recombination. Observed rate constants (k_{obs}) were obtained by nonlinear least-squares fitting of the absorbance decay curves using exponential decay functions and the Marquardt−Levinberg algorithm.

ΔA spectra were recorded at millisecond pump−probe delays using a multichannel CCD-based spectrometer. The white light source was a Xe flash lamp (pulse duration of 2 μs) that was electronically delayed from the laser photolysis flash. The ΔA spectra were obtained by referencing the delayed transmittance against that recorded with the flash lamp but without laser photolysis. The temperature of the photolyzed sample was monitored with a fine Fe:constantan thermocouple (TC), which was inserted into the sample cell such that the TC junction was positioned in the center of the overlapping photolysis and probe beams.

There was no evidence of either thermal or photochemical damage to the samples over the course of the CO recombination experiments described herein. Steady state absorbance spectra were recorded between 350 and 750 nm immediately before and after the photolysis experiments to verify sample integrity using the same spectrophotometer described in the preceding paragraph.

*Molecular Weight Distribution. Rm*FixL* and *Rm*FixLN molecular mass determinations were accomplished by HPLC size exclusion chromatography (Bio-Rad Bio sil SEC-125 column, 1.0 mL/min flow rate, 20 min run time). Absorbance of column effluent was monitored at 398 nm for the *Rm*FixL protein runs. For column calibration, the absorbance was monitored at 280 nm. Molecular mass standards were thyroglobin, immunoglobin G, albumin, myoglobin, and B_{12}.

Native gels were prepared according to published methods (*19*). The gels were run at 4 °C over a period of 8 h. Oxygen adducts of the *Rm*FixL proteins were obtained by exposing the deoxy protein prepared in the presence of β-mercaptoethanol to oxygen. Since it has been shown that β-mercap-

toethanol slows the rate of oxy*Rm*FixL autoxidation to ferric *Rm*FixL (*6*), it was used here to maintain the hemes in their oxy form during the electrophoresis. The met derivatives were not exposed to β-mercaptoethanol prior to or during electrophoresis. After being fixed in 10% acetic acid, the gels were stained with dimethoxybenzidine (DMB) (*20*) to detect heme-containing protein. Control gels were stained with Commassie blue.

RESULTS

Kinetics of CO Recombination. In heme−CO photolysis experiments, the heme/CO geminate pair, wherein the Fe−CO bond is broken but CO remains in the heme pocket, is generated immediately upon photolysis. Geminate recombination rates are not dependent on CO concentration. Since the rates of all recombination reactions observed in this study were dependent on CO concentration (see below), none of the relaxations reported here can be attributed to geminate recombination. Hence, in the cases of *Rm*FixLN/CO and *Rm*FixL*/CO, recombination of the geminate pair is either (a) too fast to be observed with the experimental setup described above or (b) too slow to compete effectively with escape of CO from the heme pocket. For the *Rm*FixLN−CO and *Rm*FixL*−CO adducts, the total second-order recombination yields at saturating pulse energies were 0.86 and 0.73, respectively. Since the quantum yield for heme−CO photolysis is generally close to 1, geminate recombination likely accounts for the remaining fraction of the photolyzed heme and occurs at rates too fast to be observed under the experimental conditions used in this study. Hence, the recombination reactions reported here can be represented by eq 1.

$$\textit{Rm}\text{FixL} + \text{CO} \underset{k'_{\text{off}}}{\overset{k_{\text{on}}}{\rightleftharpoons}} \textit{Rm}\text{FixL}-\text{CO} \qquad (1)$$

Expressions for the rate of *Rm*FixL disappearance are given in eqs 2−5. They reveal that the rate of CO rebinding depends on the rates of both CO association (governed by k_{on}) and CO dissociation (governed by the apparent k_{off}, k'_{off}, which includes a contribution from *Rm*FixL−CO photolysis by the probe beam). Derivation of eq 3 is given in the Appendix.

$$\text{rate} = k_{\text{on}}[\textit{Rm}\text{FixL}][\text{CO}] - k'_{\text{off}}[\textit{Rm}\text{FixL}-\text{CO}] \qquad (2)$$

$$\text{rate} = (k_{\text{on}}[\text{CO}] + k'_{\text{off}})[\textit{Rm}\text{FixL}] \qquad (3)$$

$$\text{rate} = k_{\text{obs}}[\textit{Rm}\text{FixL}] \qquad (4)$$

$$k_{\text{obs}} = k_{\text{on}}[\text{CO}] + k'_{\text{off}} \qquad (5)$$

The UV−visible absorption spectra of deoxy*Rm*FixL* and its CO adduct are compared in the inset of Figure 1. Spectra for deoxy*Rm*FixLN and its CO adduct are comparable (data not shown). Figure 1 also shows the 440 nm transient absorbance (TA) traces for rebinding of CO to photogenerated deoxy*Rm*FixL* and deoxy*Rm*FixLN acquired with CO in large excess (pseudo-first-order conditions). Relaxation of the ΔA signal was monitored at 440 nm because it is the wavelength of maximum absorptivity difference, $\Delta\Delta_{max}$, between *Rm*FixL−CO derivatives and their photoproducts. Fitting of ΔA relaxation data acquired under these conditions yields observed rate constants, k_{obs}, and the ΔA amplitudes for the relaxation processes.

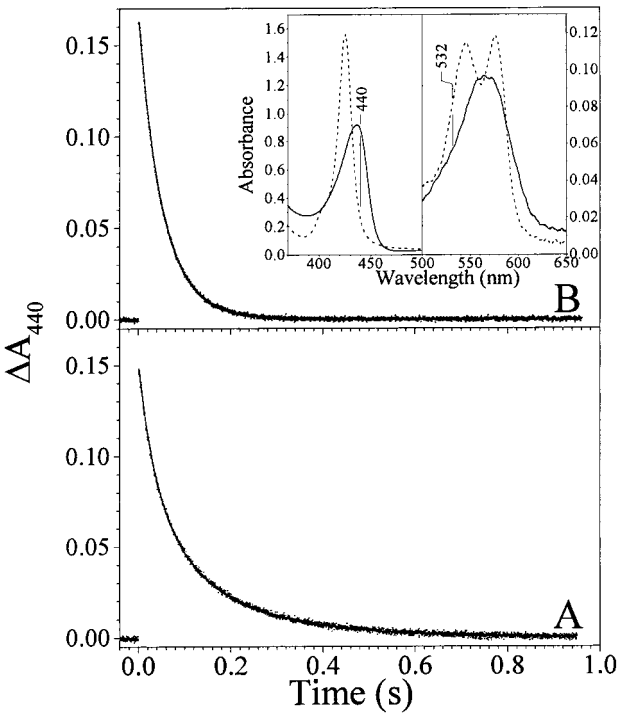

FIGURE 1: Transient absorbance change observed upon flash photolysis of CO from the *Rm*FixL−CO adduct. The rapid increase in absorbance at 440 nm is associated with CO dissociation from the heme. (A) CO recombination with *Rm*FixL* tracked by monitoring ΔA_{440} with time. (B) CO recombination with *Rm*FixLN tracked by monitoring ΔA_{440} with time. Data are shown as points. The data were fit to a two-term exponential function for *Rm*FixL* (60 μM) and a single-term exponential function for *Rm*FixLN (57 μM). The fits are shown as solid lines. Both samples were under 1 atm of CO. The inset shows visible spectra of the *Rm*FixL*−CO adduct (thick line) and deoxy*Rm*FixL* (thin line). The CO was photolyzed with a 3 ns pulse of 532 nm laser light (25 mJ/pulse).

CO recombination to *Rm*FixL* is characterized by two kinetic phases. Lifetimes (τ) and amplitudes (ΔA) of these phases were obtained by fitting the TA traces to a two-term exponential function of the form $\Delta A_{total} = \Delta A_{fast} \exp(-t/\tau_{fast}) + \Delta A_{slow} \exp(-t/\tau_{slow})$. Under 1 atm of CO at 24.5 °C, the observed *Rm*FixL*−CO recombination rate constants ($k_{obs} = \tau^{-1}$) were 26.1 ± 0.2 and 8.69 ± 0.07 s^{-1}. As expected for k_{obs} formulated as in eq 5, Figure 2 shows that both observed rate constants are independent of [*Rm*FixL*]. Thus, the recombination reactions are first-order in [*Rm*FixL*] according to eq 4. Since oxygen binding to *Rm*FixL has been shown to be noncooperative (*21*), it is likely that CO binding is also noncooperative. These two kinetic phases are attributed to CO recombination with two interconvertible *Rm*FixL* conformers, **I** (fast) and **II** (slow), which will be discussed below.

CO recombination to *Rm*FixLN is a single-phase process, as judged by the quality of the fit to a single-exponential function shown in Figure 1. As with *Rm*FixL*, the k_{obs} (25.8 ± 0.2 s^{-1}, 24.5 °C) was independent of [*Rm*FixLN], indicating that *Rm*FixLN−CO recombination is also first-order in [*Rm*FixLN] (data not shown).

The apparent dissociation rate constant, k'_{off}, has contributions from (a) thermal CO dissociation (k_{off}) and (b) photolysis of the *Rm*FixL−CO adduct by the 440 nm probe

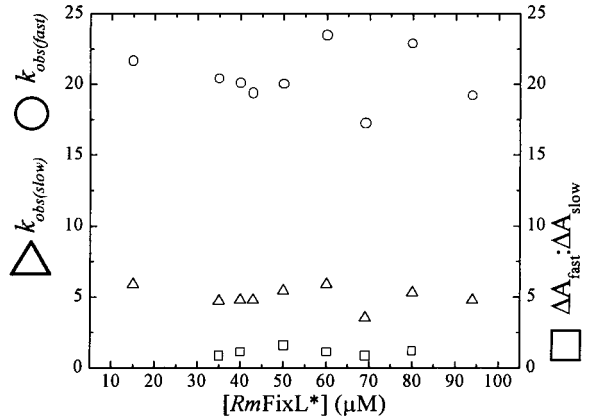

FIGURE 2: Plots of $k_{obs(fast)}$ and $k_{obs(slow)}$, as a function of [*Rm*FixL*] indicate that, under pseudo-first-order conditions, both recombination pathways are first-order in protein concentration. ΔA_{fast} and ΔA_{slow} were obtained directly from exponential fits of the TA data. Since the ΔA_{fast}:ΔA_{slow} ratio is independent of [*Rm*FixL*], the interconversion of conformers **I** and **II** is also first-order in [*Rm*FixL*].

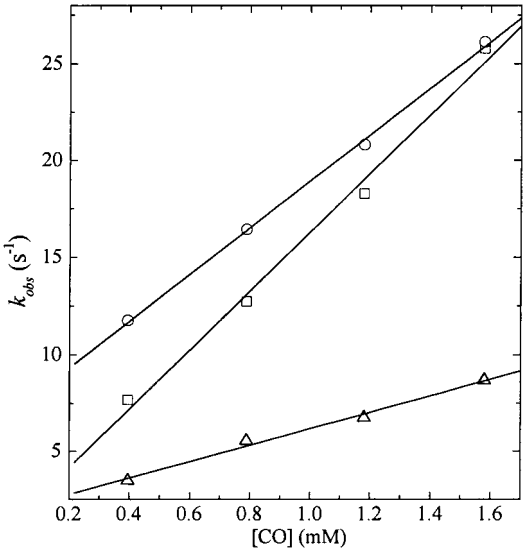

FIGURE 3: k_{obs} as a function of CO concentration. The experiments were carried out under psuedo-first-order conditions at 1 atm and 24.5 °C. Values of k_{obs} were determined from the exponential fits of ΔA_{440} vs time for *Rm*FixL* (two-term exponential function) and *Rm*FixLN (single-term exponential function). The solid lines represent the best fits to the experimental data. The k_{obs} values are represented as follows: (□) *Rm*FixLN, (○) *Rm*FixL* fast phase, and (△) *Rm*FixL* slow phase.

beam (k_{phot}). As shown in Figure 3, plots of k_{obs} versus [CO] are linear for both *Rm*FixL* and *Rm*FixLN. Values for k_{on} and k'_{off} for CO recombination with *Rm*FixLN and *Rm*FixL* were determined from the slopes and the *y*-intercepts of these plots and are listed in Table 1. To maintain consistency in notation with Table 1, k'_{off} is hereafter formulated as $k_1 + k_{phot}$ for the fast recombination phase and as $k_{-5} + k_{phot}$ for the slow phase. The linear dependence of the observed rate constants upon [CO] indicates that all recombination reactions monitored here involve a second-order step. Values of $k_1 + k_{phot}$ and $k_{-5} + k_{phot}$ listed in Table 1 are considerably larger than the thermal dissociation rate constant previously reported ($k_{off} = 0.083\ s^{-1}$) (*21*). The difference is attributed to CO photolysis by the probe beam.

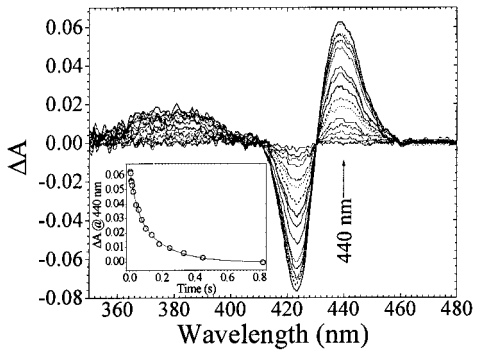

FIGURE 4: Transient Δ*A* spectra showing CO recombination with photolyzed (*Rm*FixL*)$_2$ at room temperature. Spectra were recorded at delays ranging from 10 to 800 ms and were referenced against the spectrum of (*Rm*FixL*−CO)$_2$. [*Rm*FixL*−CO] = 15 μM, and [CO] = 1.58 mM. The inset shows ΔA_{440} vs time. Open circles are original data points obtained from the TA spectra shown. The solid line is the fit of the data points to a two-term exponential function (same as that used in Figure 1).

Photodissociation of the *Rm*FixLN−CO and *Rm*FixL*−CO adducts exhibited similar photolysis saturation behavior. The ΔA_{440} after photolysis is dependent on the pulse energy used to photodissociate the sample. For pulse energies of ≥20 mJ, photolysis of the *Rm*FixLN−CO and *Rm*FixL*−CO adducts was saturated; higher energies did not increase the second-order recombination yield, as judged by ΔA_{440} (data not shown). Under saturating photolysis conditions, a larger ΔA_{440} is observed for *Rm*FixLN than for *Rm*FixL*. In these experiments, ΔA_{440} corresponds to the amount of 5-c HS heme that persists after the photolysis pulse due to CO having diffused out of the heme pocket. If comparable photolysis quantum yields are assumed, the rate of geminate CO recombination competes with CO escape from the pocket more effectively in *Rm*FixL* than in *Rm*FixLN.

Figure 4 shows Δ*A* spectra in the B-band region of *Rm*FixL*. They show a monotonic decay in Δ*A* intensity across the entire spectrum with increasing delay between laser-induced CO photolysis and white light probe pulses from a 2 μs Xe flash lamp. For comparison with Figure 1, the inset shows the ΔA_{440} decay along with the best fit line for the same two-term exponential decay function used for the fit shown in Figure 1. The spectra exhibit clean isosbestic behavior, indicating that interconversion of **I** and **II** does not cause detectable spectral changes in the deoxy heme. This is consistent with the conformational transition occurring

Table 1: Rate Constants for CO Recombination with *Rm*FixL[a]

protein	$k_1 + k_{phot}$ (s^{-1})[b]	k_{-2} ($M^{-1}\ s^{-1}$)[c]	k_3 (s^{-1})	k_4 ($M^{-1}\ s^{-1}$)[d]	$k_5 + k_{phot}$ (s^{-1})[e]	k_6 (s^{-1})
*Rm*FixLN (heme domain)	1 ± 1	$(1.5 \pm 0.1) \times 10^4$	N/A	N/A	N/A	N/A
*Rm*FixL* (heme−kinase)	6.9 ± 0.4	$(1.20 \pm 0.03) \times 10^4$	13.5	$(4.2 \pm 0.3) \times 10^3$	1.9 ± 0.3	3.3

[a] Uncertainties are ±10% where not indicated. Rate measurements were taken at 24.5 °C. [b] This sum is k'_{off} for CO recombination with **I**. [c] The rate constant for CO binding to **I** corresponds to k_{on} in the general kinetic expression given in eq 5. [d] The rate constant for CO binding to **II** corresponds to k_{on} in the general kinetic expression given in eq 5. [e] This sum is k'_{off} for CO recombination with **II**.

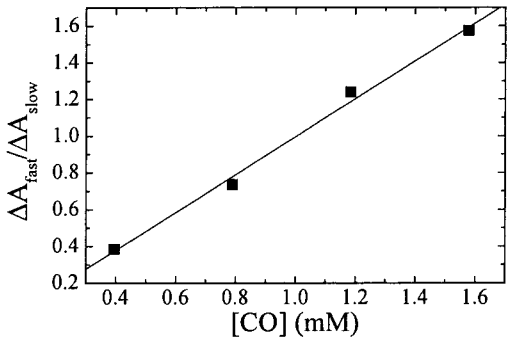

FIGURE 5: Dependence of the ΔA_{fast}:ΔA_{slow} ratio on [CO] for *Rm*FixL* recombination. ΔA_{fast} and ΔA_{slow} were obtained directly from fits to a two-term exponential decay function. As [CO] is increased, the ΔA_{fast}:ΔA_{slow} ratio increases because the fast recombination that is dependent on [CO] (**I** + CO) competes more effectively with the conversion to **II** that is independent of [CO].

sufficiently far from the heme that its electronic properties are not strongly affected.

Without a spectral change, neither the rate of interconversion between forms **I** and **II** of *Rm*FixL* nor its dependences upon protein and ligand concentrations can be determined directly from recombination rates. To gain these mechanistic insights, it was necessary to determine the effects of reactant concentrations on the ΔA_{fast}:ΔA_{slow} ratio. Among the simplest mechanisms to explain the interconversion is (a) a unimolecular conformational transition or (b) a bimolecular protein−protein association reaction. If the interconversion is rate limited by protein−protein association, then increasing the protein concentration would cause conversion of **I** to **II** to compete more effectively with direct recombination to **I**, thereby increasing ΔA_{slow} at the expense of ΔA_{fast}. Figure 2 shows that, at room temperature, the ΔA_{fast}:ΔA_{slow} ratio equals 1.4 and is independent of [*Rm*FixL*], indicating that formation of **II** is first-order in [*Rm*FixL*] and cannot be rate limited by a protein association step. On the other hand, the ΔA_{fast}:ΔA_{slow} ratio should increase in response to increasing [CO] because the rate of direct recombination to **I** would be increased without affecting the unimolecular conversion to **II**. As expected for a fast [CO] dependent recombination to **I** and a [CO] independent conversion of **I** to **II**, the ΔA_{fast}:ΔA_{slow} ratio depends linearly upon [CO]. Figure 5 shows that the ΔA_{fast}:ΔA_{slow} ratio doubles with a doubling of [CO]. Hence, the **I** to **II** conversion is unimolecular and does not involve CO. Since the recombination with **I** and the conversion of **I** to **II** are competing processes, their relative rates are indicated by the ratio of ΔA amplitudes (ΔA_{fast}:ΔA_{slow}). Since both processes exhibit a first-order dependence on [*Rm*FixL*], an estimate of the interconversion rate constant can be made by dividing the k_{obs} for **I** recombination (k_{-2}[CO], Table 1) by $\Delta A_{fast}/\Delta A_{slow}$. This rate constant is listed in Table 1 as k_3.

Effects of the Photolysis Repetition Rate. During the course of this study, it became apparent that the shape of the *Rm*FixL* rebinding curve depends on the photolysis repetition rate. Plots of ln ΔA_{440} versus time for different photolysis recycle times are shown in Figure 6. The breaks in the log plots for *Rm*FixL* recombination in parts IA and IB of Figure 6 are consistent with recombination to the two aforementioned species, **I** and **II**. With increasing repetition rates (Figure 6I, A → B → C → D), there is a significant

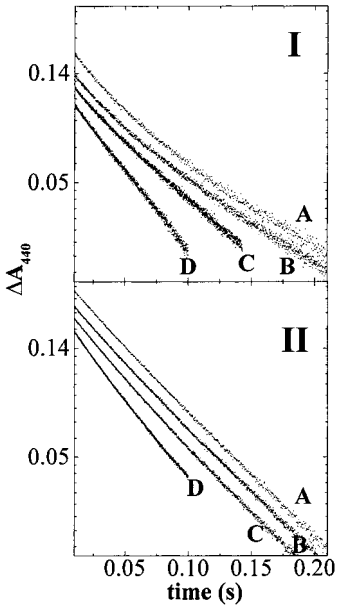

FIGURE 6: Effect of photolysis pulse repetition rate on CO recombination with *Rm*FixLs. (I) Plots of ln(ΔA_{440}) vs time for *Rm*FixL* at (A) 0.5, (B) 3, (C) 7, and (D) 10 Hz. The *Rm*FixL* concentration is 60 μM. Pulse energy = 20 mJ at sample; P_{CO} = 1 atm. (II) Plots of ln(ΔA_{440}) versus time for *Rm*FixLN at (A) 0.5, (B) 2, (C) 5, and (D) 10 Hz. The 65 μM *Rm*FixLN sample was under 1 atm of CO. Pulse energy = 25 mJ at sample. Data sets B−D have been offset from data set A on the ΔA_{440} axis of panels I and II for clarity of viewing.

but reversible change in the shape of ln ΔA_{440} versus time. The plots for *Rm*FixL*−CO recombination show its biphasic behavior at low repetition rates (parts IA and IB of Figure 6). With a photolysis repetition rate of 7 Hz (part IC of Figure 6), the plot is nearly linear, but quality fits of the data still required two-term exponential functions. At a still higher pulse repetition rate (i.e., ≥10 Hz, part ID of Figure 6), the plot is virtually linear, suggesting that only one recombination pathway is left operating at short recycle times. There is no significant change in the shape of ΔA_{440} decay curves for *Rm*FixLN as the photolysis pulse repetition rate is increased. At all repetition rates that were investigated, CO recombination for *Rm*FixLN proceeds via a single pathway (panel II of Figure 6). Both proteins exhibit increases in k_{obs} with increasing repetition rate, as seen by the increased negative slopes in Figure 6.

The repetition rate dependence of ΔA_{fast} and ΔA_{slow} suggested that there is a *Rm*FixL* relaxation process occurring after CO rebinding. There is no measurable UV−visible spectral change associated with this relaxation, but if it is not allowed to proceed to completion before the next photolysis pulse, ΔA_{fast} and ΔA_{slow} do not have their characteristic low repetition rate amplitudes. Hence, we set out to exploit the repetition rate dependence of ΔA_{fast} and ΔA_{slow} to characterize this nonspectral relaxation. Characterization was complicated by laser-induced thermal effects that first had to be clarified.

Thermal Effects at High Photolysis Repetition Rates. Figures 6 and 7 show two effects of the photolysis laser flash on sample temperature. The first is a dependence of the steady state sample temperature (measured directly in the laser beam cross section) on repetition rate. This dependence is seen by their linear relationship in Figure 7A. The increase

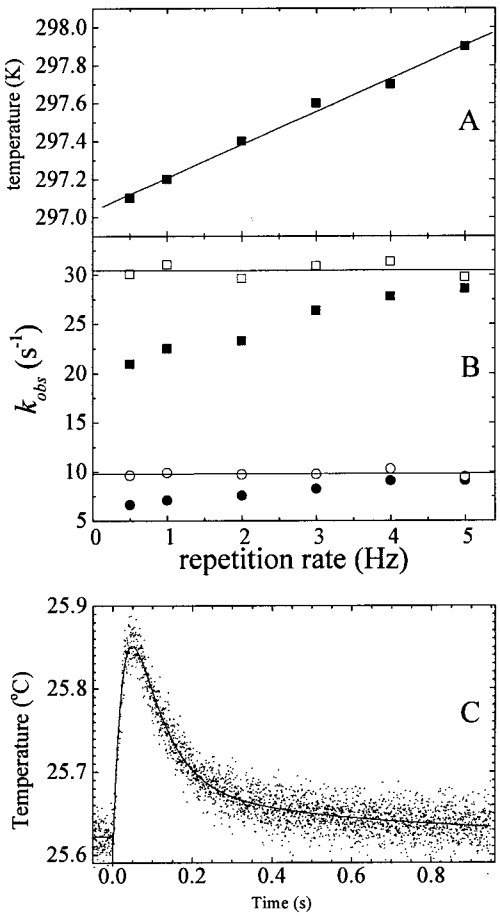

FIGURE 7: (A) Sample temperature as a function of photolysis pulse repetition rate. Pulse energy = 30 mJ at the sample. [*Rm*FixL*−CO] = 60 μM (■). P_{CO} = 1 atm. Initial sample temperature = 22.8 °C. (B) k_{obs} for CO recombination vs photolysis pulse repetition rate. Values for k_{obs} were obtained by fitting ΔA_{440} vs time to a two-term exponential decay function for the *Rm*FixL*−CO adduct. Values of k'_{obs} were obtained by correcting the k_{obs} for laser-induced temperature increases using activation energies. Solid lines are the best linear fits to the data: (■) k_{obs} for recombination with **I**, (□) k'_{obs} at 24.8 °C for recombination with **I**, (●) k_{obs} for recombination with **II**, and (○) k'_{obs} at 24.8 °C for recombination with **II**. (C) Temperature vs time after the laser flash. Points are actual data, and the solid line is the best fit to a two-term exponential function to model the rise and fall of the sample temperature in the laser beam cross section.

in steady state temperature is manifested in increased rate constants, as seen by the increased negative slopes in Figure 6 at higher repetition rates.

To compare the rate constants obtained from low- and high-repetition rate experiments with *Rm*FixL*, it was necessary to determine their temperature dependencies. The observed rate constants, k_{obs}, for both recombination phases exhibited Arrhenius behavior, and their activation energies were determined from the slopes of Arrhenius plots (ln k_{obs} vs T^{-1}). These activation energies, E_{fast} (226 kJ/mol) and E_{slow} (319 kJ/mol), were used to correct the measured rate constants, k_{obs}, for the laser-induced temperature increases at higher repetition rates (k'_{obs}). Figure 7B shows that the corrected rate constants for both phases are independent of repetition rate and verifies that increases in k_{obs} with repetition rate are actually due to the increased temperature caused by dissipation of more pump laser energy at the higher repetition rates.

The second effect of the laser photolysis flash on sample temperature is transient in nature, as shown in Figure 7C. This transient increase in temperature was measured directly in the beam cross section using the aforementioned TC. The TC signal was connected directly to a digital sampling oscilloscope using a 1 MΩ input impedance. Even though the time dependence of temperature in Figure 7C is distorted by the large RC time constant of the high-impedance TC circuit, a transient temperature increase of a few tenths of a degree is clearly evident. Consequently, the rate constants determined under these conditions increase slightly immediately after the laser flash and decrease during the CO recombination due to dissipation of thermal energy from the beam cross section. The time constant for this dissipation was estimated to be 0.12 s by exponential fitting of the data in Figure 7C. Graphically, this temperature transient manifests itself as a very slight deviation from linearity in the log plots, which is evident upon careful inspection of part ID of Figure 6 but is most evident in panel II of Figure 6 because of the higher signal-to-noise ratio (*S*/*N*). In many CO photolysis studies, the effects of this temperature transient are not seen because the rates of recombination are much faster than that of the dissipation of energy from the laser flash. It is observed here because the CO recombinations occur on the same time scale as thermal dissipation. With the thermal effects of the photolysis laser now clarified, it was possible to proceed with characterizing the slow spectrally silent relaxation discussed above.

Recovery of the Equilibrium RmFixL−CO Adduct.* ΔA_{440} and k_{obs} for both *Rm*FixL*−CO recombination phases were independent of photolysis pulse repetition rate between 0.1 and 1 Hz. However, at repetition rates of >1 Hz, the amplitude of the slow phase (ΔA_{slow}) increased at the expense of ΔA_{fast} due to buildup of **II** (Figure 8). At >7 Hz, only the slow phase was observed. Figure 8B shows the recovery of ΔA_{fast} with increased time between pulses (recycle time). This curve shows that for recycle times of ≥1 s, the system is at equilibrium when CO photolysis is induced. The ΔA_{440} decay curves at intermediate repetition rates show the buildup of the conformationally unrelaxed *Rm*FixL*−CO adduct, the extent of which depends inversely upon recycle time. This buildup is completely reversible; that is, increasing the recycle time to >1 s returns the ΔA_{fast}:ΔA_{slow} ratio to its equilibrium value of 1.4. Figure 8A shows that ΔA_{total} decreases slightly with decreasing recycle time. This small effect could arise either from a slightly diminished second-order quantum yield for the conformationally unrelaxed *Rm*FixL*−CO adduct or from a slight buildup of deoxy*Rm*-FixL* that persists between photolysis cycles. In either case, CO binding to the heme does not cause rapid back conversion of conformation **II** to conformation **I**. Inducing photolysis before complete conformational relaxation yields **II** directly. These observations indicate that, although recycle time does not affect the mechanism of *Rm*FixL* recombination, it dictates which pathway dominates the process. The influence of recycle time on the interchange between the ΔA_{fast} and ΔA_{slow} amplitudes indicates that the biphasic CO recombination kinetics arise from interconvertible *Rm*FixL* conformations, rather than two uncoupled equilibrium populations giving rise to parallel recombinations.

Equilibrium Molecular Weight Distributions of RmFixL. Gel permeation HPLC and native gel electrophoresis studies

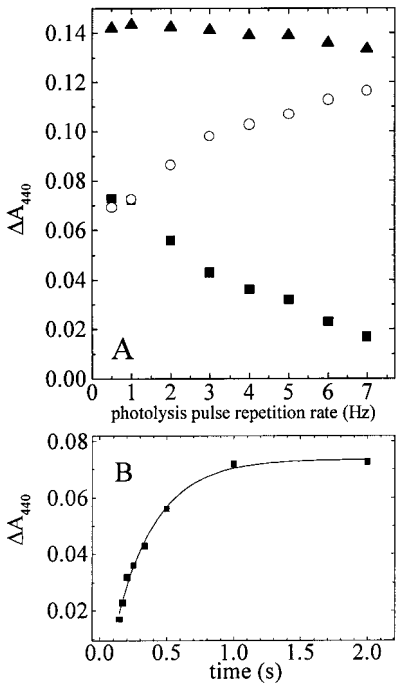

FIGURE 8: (A) ΔA_{440} for the fast (■) and slow (○) *Rm*FixL*−CO recombination phases at various photolysis pulse repetition rates. ΔA_{440} for each phase was obtained from the two-term exponential fit of the TA data at a given repetition rate. The black triangles represent the total ΔA_{440}. [*Rm*FixL*] = 60 μM, and P_{CO} = 1 atm. The 3 ns, 532 nm laser pulse energy was 20 mJ at the sample. (B) Photolysis pulse repetition rate data for the fast phase plotted as ΔA_{440} vs photolysis recycle time to determine the rate of reappearance of equilibrium of (*Rm*FixL*−CO)$_2$ after photolysis. The solid line represents a single-term exponential fit to the data.

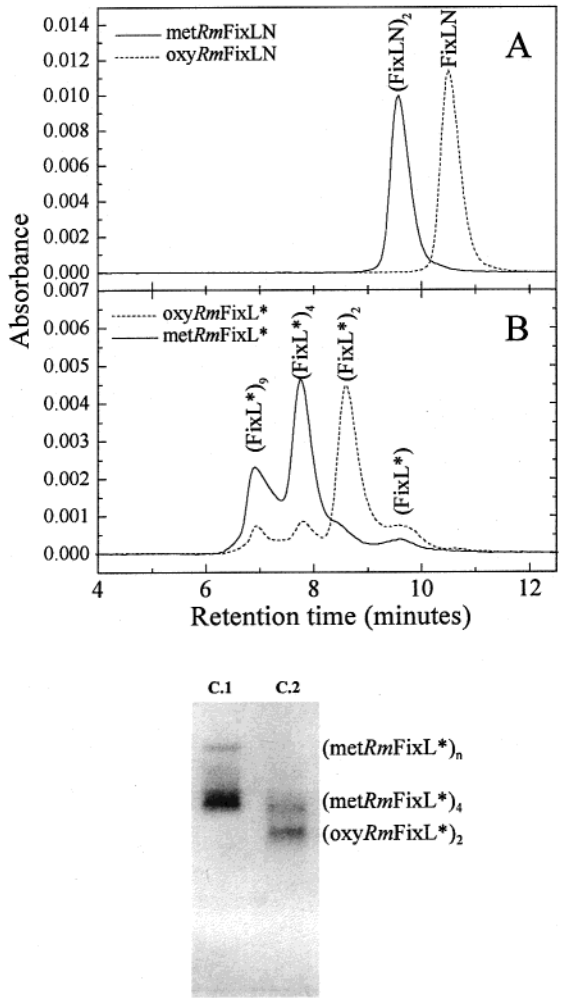

FIGURE 9: Speciation of *Rm*FixL derivatives in their oxy and met forms. HPLC gel filtration traces for (A) *Rm*FixLN and (B) *Rm*FixL*. The data were calibrated as described in Materials and Methods. (C) Native gel showing met*Rm*FixL* (C.1) and oxy*Rm*FixL* (C.2). The C.2 lane shows some met*Rm*FixL* due to autoxidation during the electrophoresis run. The gel was stained with DMB to show positions of heme-containing proteins.

reported here show that *Rm*FixLN and *Rm*FixL* self-associate in response to conversion from their oxy to their met forms. Oxy*Rm*FixLN ran as monomer on the size exclusion column, while its met form was dimeric (Figure 9A). Oxy*Rm*FixL* ran as a dimer, whereas met*Rm*FixL* was predominantly higher-order oligomers (Figure 9B). The observation of some higher molecular weight forms in the oxy*Rm*FixL* chromatographic run is consistent with small amounts of met*Rm*FixL* due to autoxidation or to a shift in the oxy/deoxy*Rm*FixL* equilibrium during the run. While the O_2 adduct is the most physiologically relevant LS form, the met form is relevant in that, like the deoxy form, it contains a 5-c HS heme and exhibits kinase activity (*6*). Relative populations of the oligomers were quantified by integration of the chromatograms in Figure 9 and are listed in Table 2.

Oxy and ferric *Rm*FixLN each run as one band on the native gel. Oxy*Rm*FixLN migrates faster on the native gel than its met counterpart. While this could be due either to differing oxy and met *Rm*FixLN conformations or to the presence of protein oligomers, the corresponding gel permeation data in Figure 9A suggest that the difference is due to dimerization of the HS met form.

The kinase-inactive oxy*Rm*FixL* migrates on the native gel as a single band (Figure 9C). However, two bands are observed for kinase-active met*Rm*FixL*. These two bands are consistent with the high-molecular weight met*Rm*FixL* oligomers observed by HPLC. The slowly migrating band corresponding to the 9-mer is substantially smaller than the more rapidly migrating band of the tetramer; this is probably the result of the long run time of the gel which favors dissociation of protein oligomers. The same set of bands was revealed with Commassie blue and DMB staining. SDS−

Table 2: *Rm*FixLN and *Rm*FixL* Oligomer Populations

protein	form[a]	kinase activity	predicted molecular mass (kDa)[b]	observed molecular mass (kDa) (% form observed)[c]
*Rm*FixLN	HS, met	none	16.1	27.6 (100)
	LS, oxy	none	16.1	17.7 (100)
*Rm*FixL*	HS, met	active	42.8	42 (8)
				96 (9)
				186 (53)
				376 (30)
	LS, oxy	inactive	42.8	42 (17)
				96 (62)
				186 (12)
				376 (9)

[a] Met derivatives were obtained by autoxidation of oxy*Rm*FixLs. Oxy forms were prepared by exposure of deoxy to O_2 in the presence of β-mercaptoethanol which helps stabilize the oxy adducts (*6*). [b] From ref *2*. [c] Populations were derived from integration of HPLC gel filtration traces.

Scheme 1: Model for CO Recombination with *Rm*FixL*

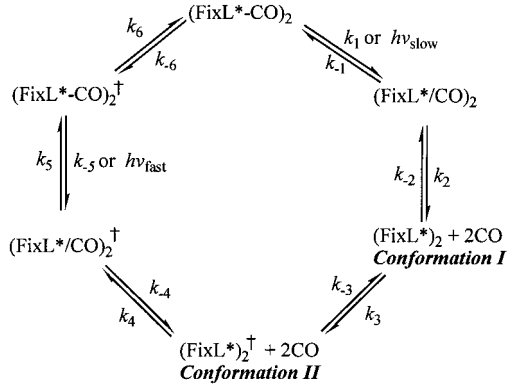

PAGE gels verified that there are no detectable protein impurities in the sample. Hence, all oligomers contain only heme-loaded *Rm*FixL*. The gel permeation and native gel data support three conclusions. (1) When the heme in *Rm*FixL* is 6-c LS (kinase inactive), the protein is primarily dimeric. (2) The dimeric form of *Rm*FixL* is converted to tetrameric and larger oligomers when its strong-field ligand is removed. (3) The lack of highly associated protein in met*Rm*FixLN suggests that stabilization of the oligomers larger than a dimer involves the kinase domain. These data do not support conclusions relating to the physiological relevance of *Rm*FixL* dimers, tetramers, and 9-mers. However, the dependence of their relative populations upon heme ligation and spin state is relevant to the interpretation of the CO recombination results reported here.

Since this study involves the CO adducts rather than the oxy form of *Rm*FixL*, it was important to know whether the CO adduct also forms oligomers. Running the chromatographic experiments anaerobically in the presence of saturating [CO] was not technically feasible with the facilities at hand. However, we have shown that the *Rm*FixL*−CO adduct and oxy*Rm*FixL* are held back to the same extent by a YM100 ultrafiltration membrane. This was determined by SDS−PAGE analysis of the respective filtrates (data not shown). The similarity in their ultrafiltration behavior suggests that the *Rm*FixL*−CO adduct and oxy*Rm*FixL* have similar molecular weight distributions.

Model for RmFixL−CO Recombination. Scheme 1 shows the proposed model for biphasic CO recombination with *Rm*FixL*. In this discussion, *Rm*FixL* indicates the deoxy protein and the rate constant subscripts refer to the corresponding mechanistic steps illustrated in Scheme 1. The 6-c LS CO-bound protein is proposed to be a dimer at equilibrium, (*Rm*FixL*−CO)$_2$, as discussed above.

Scheme 1 shows that immediately after photolysis at repetition rates of ≤1 Hz (indicated by $h\nu_{slow}$ in Scheme 1), a nonequilibrium population of the geminate pair, (*Rm*FixL*/CO)$_2$, is established. The geminate pair relaxes via two competing pathways, geminate recombination (k_{-1}) to give (*Rm*FixL*−CO)$_2$ and escape of CO from the heme pocket (k_2) to yield (*Rm*FixL*)$_2$. Even though geminate recombination is not observed on the time scale investigated here, it is evidenced by the moderate yield (30%) of total second-order CO recombination. The nonequilibrium population of (*Rm*FixL*)$_2$ has its heme−kinase interface in the ligated (kinase-inactive) conformation, which also relaxes by two pathways. One is direct CO recombination, whose rate is limited by

Scheme 2: Model for CO Recombination with *Rm*FixLN

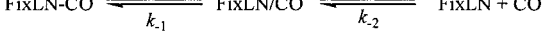

re-entry of CO into the heme pocket (k_{-2}). The sequence of events is the same up to this point for *Rm*FixLN and *Rm*FixL*. Scheme 2, which illustrates CO recombination to *Rm*FixLN, comprises a subset of the steps in Scheme 1. Similarity in both the second-order recombination yields and the direct CO recombination rate constants suggests that the kinase domain has only a slight influence on the rates of the mechanistic steps just described. However, the kinase domain causes the *Rm*FixL* and *Rm*FixLN mechanisms to diverge at this point. At a rate competitive with direct CO recombination (k_3), the presence of the kinase causes the heme−kinase domain interface to lock into an intermediate conformation, (*Rm*FixL*)$_2^\dagger$, which measurably slows (raises the barrier to) CO recombination (k_4). Since the photolysis−recombination cycle starts from the dimer, (*Rm*FixL*−CO)$_2$, and since conversion to (*Rm*FixL*)$_2^\dagger$ is independent of [*Rm*FixL*], the interconversion is concluded to be first-order in [*Rm*FixL*]. Furthermore, for reasons explained below, it is concluded to be an intradimer conformational transition.

The kinase-dependent conformational transition is hypothesized to be a heme → kinase signal transmission event. As such, it may be the prelude to clustering of dimers into larger equilibrium 5-c HS oligomers (Figure 9) that would form if CO were not present to reverse progress along the clustering pathway by rebinding to the heme.

The rate of reversal of this putative signal transduction pathway is revealed in the dependence of ΔA_{fast} (due to CO recombination with **I**) on photolysis repetition rate. With high repetition rates, there is insufficient time for (*Rm*FixL*−CO)$_2^\dagger$ to relax to its equilibrium form, (*Rm*FixL*−CO)$_2$, and a buildup of (*Rm*FixL*−CO)$_2^\dagger$ is observed. Subsequent photolysis at a high repetition rate (indicated by $h\nu_{fast}$ in Scheme 1) produces (*Rm*FixL*)$_2^\dagger$ directly, and at repetition rates of ≥7 Hz, only recombination to (*Rm*FixL*)$_2^\dagger$ was observed, as evidenced by its temperature-compensated k'_{obs}. Given that k_{-3} is small relative to k_4, photolysis of (*Rm*FixL*−CO)$_2$ is the only means of producing significant amounts of **I**. Hence, the rate of change in ΔA_{fast} with increasing recycle time (Figure 8B) reports the rate at which (*Rm*FixL*−CO)$_2$ is repopulated by relaxation of (*Rm*FixL*−CO)$_2^\dagger$ (k_6). This relaxation rate constant (k_6) was estimated by fitting ΔA_{fast} versus recycle time to a single-term exponential function (Table 1). This rate constant is independent of [*Rm*FixL*] (data not shown), indicating that relaxation of the species formulated as (*Rm*FixL*−CO)$_2^\dagger$ in Scheme 1 is an intraspecies process. In other words, the transformation of **I** to **II** (k_3) cannot be a dimer dissociation, which is not surprising given that equilibrium chromatography shows that solutions of unligated forms of *Rm*FixL* comprise higher molecular weight oligomers than their ligated counterparts (Figure 9). Since the conversion of **I** to **II** is first-order in *Rm*FixL* and does not produce monomers, we conclude it is an intradimer conformational transition.

In this discussion of the mechanism illustrated in Scheme 1, it is assumed that recombination of the geminate pair, (*Rm*FixL*/CO)$_2^\dagger$ (k_5), is much faster than entry of CO into the heme pocket of (*Rm*FixL*)$_2^\dagger$ (k_4). Under this assumption,

the rate of (*Rm*FixL*−CO)$_2^\dagger$ formation is limited by formation of the geminate pair.

Although there is no evidence for cooperative CO binding, the dimeric nature of the *Rm*FixL*−CO adduct presents the possibility for cooperativity. Hence, we needed to determine whether the slow phase was a quaternary-type transition between the constituent *Rm*FixL* monomers of (*Rm*FixL*)$_2$. This was accomplished by assessing the CO recombination with nonsaturating photolysis pulse energies. Under these conditions, *Rm*FixL* still exhibited biphasic kinetics with the same rate constants observed with saturating photolysis energies. This suggests that neither recombination phase can be attributed to communication between hemes of different *Rm*FixL* molecules and is consistent with a lack of cooperativity in CO binding.

Scheme 2 shows the model for CO rebinding to *Rm*FixLN. On the basis of rate constants, the recombination of CO with *Rm*FixLN is similar to that for the fast phase of (*Rm*FixL*)$_2$. After photolysis of the *Rm*FixLN heme, the Fe(II) center becomes 5-c and HS. Although gel filtration and dynamic light scattering studies (*8*) indicate that the 5-c HS *Rm*FixL heme domain is dimeric, the CO recombination kinetics model does not require a dimerization step. This suggests that *Rm*FixLN does not dimerize at a rate competitive with CO rebinding to the monomer.

DISCUSSION

Single-phase CO recombination kinetics have been reported previously for *Rm*FixLT (a different heme−kinase construct) and *Rm*FixLH (a different heme domain construct) (*21*). The reported rate constants ($k_{on} = 1.2 \times 10^4$ and 1.7×10^4 M^{-1} s^{-1}, respectively) are similar to those reported here for *Rm*FixL* and *Rm*FixLN. It is not clear why two rebinding phases were not observed for *Rm*FixLT in the earlier study. Given that the recombination is slow, it is possible that ΔA was not monitored for a sufficient length of time to measure the change in rebinding rate reported here for *Rm*FixL*. Another possible explanation is that CO photolysis was carried out at a repetition rate of 10 Hz where many Q-switched Nd:YAG lasers operate. As shown above, only one phase is observed at 10 Hz (Figure 6). Though it seems unlikely, the possibility that the second recombination phase is unique to the *Rm*FixL* construct cannot be eliminated at this point.

Slow ligand binding to *Rm*FixL relative to hemoglobin A (HbA) and other heme proteins is one of its hallmarks (*7*, *21*). Additionally, the results reported here set it apart from HbA in yet another respect. Whereas the HbA quaternary R → T transition occurs with a lifetime ($\tau = k^{-1}$) of only 20 μs (*22*), the putative heme kinase signaling transition reported here for *Rm*FixL* occurs more than 3 orders of magnitude slower with a lifetime of 50 ms. Since the structure of the kinase domain has not been reported, it is difficult to rationalize this large difference in detailed structural terms. However, given that the only significant protein conformational change between liganded and unliganded forms of the *Bj*FixL heme domain occurs in the flexible FG loop, perhaps the flexibility of the loop plays an important role in determining the rate of signal transmission by virtue of having the flexibility to sample a large conformational space. If the loop is sufficiently flexible to have many nearly-degenerate conformations, the time required to search the conformational space accessible by the loop could have the effect of slowing the transition.

The differences in the CO recombination kinetics of *Rm*FixLN and *Rm*FixL* indicate that heme ligand binding and release are energetically coupled to the conformation of the kinase domain. Moreover, the conformational interconversion between (*Rm*FixL*)$_2$ and (*Rm*FixL*)$_2^\dagger$ alters the rate of CO binding to the heme. We propose that (*Rm*FixL*)$_2^\dagger$ is a switching intermediate whose formation requires an interdomain conformational transition. We further postulate that this conformation (**II**) disposes HS (*Rm*FixL*)$_2$ toward formation of the tetrameric and higher oligomers that are present at equilibrium. Even if more extensively aggregated forms of HS *Rm*FixL* are not physiologically relevant, they are converted to (*Rm*FixL*)$_2$ upon binding of O_2 and probably upon binding of CO. At the very least, this suggests conformational differences between activated and inhibited *Rm*FixL* that result in different surface interactions between *Rm*FixL* units. Since these protein−protein interactions are modulated by the same heme parameters as kinase activity, namely, coordination number and spin state, the possibility that such interactions are mechanistically relevant cannot be discounted.

The oligomers of met*Rm*FixL* (and ostensibly, deoxy*Rm*FixL*) may be physiologically important. Evidence from a number of two-component regulatory systems comprising histidine kinases homologous with the kinase domain of *Rm*FixL supports signal transduction mechanisms involving dimerization and cross phosphorylation (*23*−*26*). It is noteworthy that in *Rm*FixL, the O_2 receptor and histidine kinase functions are harbored by the same protein. Studies of the aspartate and serine receptors in chemotaxis indicate that these membrane-bound receptors exist as dimers and form complexes with the histidine kinase, CheA (*26*−*28*). Numerous models for clustering of these dimeric receptors to communicate the binding of an effector ligand to a larger array of receptor molecules have been proposed (*30*−*32*). In vitro receptor cytoplasmic domain fragments form higher-order oligomers (*33*, *34*). The cytoplasmic domain of the serine receptor forms a trimer of dimers in solution. However, the occurrence of this oligomerization in the membrane-bound receptor has not been demonstrated (*27*). Data for the aspartate receptor indicate that interactions between a number of coupled receptor dimers can account for the limited cooperativity observed in the attractant-response curve (*35*). Receptor clustering has also been suggested for tyrosine kinase-linked receptors (*36*), suggesting that clustering may be a recurring feature in receptor signaling systems.

Reports of varying extents of *Rm*FixL heme domain aggregation have appeared in the literature. On the basis of dynamic light scattering measurements and crystallography, Miyatake and co-workers (*8*) have reported that the heme domain of *Rm*FixL is dimeric when the heme is in its ferric and deoxy states. Using gel filtration to estimate molecular masses, it has been reported that the heme domain of *Rm*FixL is monomeric (*21*). Our observation of dimeric met*Rm*FixLN and monomeric oxy*Rm*FixLN in gel permeation chromatography experiments shows that the extent of *Rm*FixLN association depends on the ligation state of the heme.

Crystals of the dimeric *Rm*FixL heme domain are reportedly reduced by soaking in sodium dithionite. However,

exposure of the ferric crystals to heme ligands such as O_2, CO, and CN^- caused the crystals to dissolve (*13*). Based upon the sensitivity of *Rm*FixLN association to the state of the heme, the following explanation is proposed. In the ferric form, the protein is in the kinase-activating conformation. Reduction of the heme leaves the heme domain in this active conformation. No conformational change or dissociation ensues; hence, the crystals remain intact. Conversion to a kinase-inactivating 6-c LS heme form causes a change in protein conformation that favors dissociation of heme domain dimers, resulting in dissolution of the crystals.

The extent of *Rm*FixL* association also depends on the heme state. When the heme is O_2-bound, the protein is dimeric, (oxy*Rm*FixL*)$_2$. This dimeric oxy form is supported by the data presented here and by a previously reported gel permeation chromatography experiment wherein *Rm*FixL* was kept in 10 mM β-mercaptoethanol (*21*), which stabilizes the oxy form. The HPLC gel permeation data presented here indicate that a kinase-activating met*Rm*FixL* form exists largely as (met*Rm*FixL*)$_4$. This is consistent with the dynamic light scattering measurements on the met heme−kinase protein which showed a broad distribution of molecular mass (*17*), suggesting the presence of oligomers in solution. Since both met*Rm*FixL and deoxy*Rm*FixL are kinase active, it is likely that deoxy*Rm*FixL* and met*Rm*-FixL* exhibit similar molecular weight distributions in solution. Native gels of cell extracts containing *Rm*FixL* have been reported to exhibit two bands. Once the protein was purified, only one band was observed (*2*). By the end of the purification process, especially if the protein is kept in β-mercaptoethanol, the heme is predominantly in its oxy form. This is consistent with the native gel reported here (Figure 9C).

Signal Transduction Model. When the kinetic and equilibrium data presented here are considered with previous structural and spectroscopic characterization of *Rm*FixL, the following sequence of signal transduction events emerges for activation of the kinase domain: (1) release of O_2 from LS oxy*Rm*FixL yields HS 5-c deoxy*Rm*FixL (*2*, *4*), (2) kinase-independent translocation of the heme iron toward the proximal His releases tension on the Fe−His bond (*11*), (3) interdomain protein conformational change occurs in response to relaxation of both proximal Fe−His tension and steric interactions with the ligand in the distal heme pocket (*7*, *9*, *15*, *16*), (4) oligomerization of *Rm*FixL in response to the ligand-coupled protein conformational change possibly brings kinase domains into sufficiently close contact for cross phosphorylation, and (5) reaction of the kinase with ATP to phosphorylate His285 (*37*).

ACKNOWLEDGMENT

We express gratitude to Professor Frank Rusnak for providing access to his HPLC facilities.

APPENDIX

Derivation of the relationship between k_{obs}, k_{on}, and k_{off} for second-order CO recombination.

$$\mathit{Rm}\text{FixL} + \text{CO} \underset{k_{off}}{\overset{k_{on}}{\rightleftharpoons}} \mathit{Rm}\text{FixL}-\text{CO} \tag{A1}$$

where

$$[\text{CO}] \gg [\text{FixL}] \tag{A2}$$

$$K = \frac{k_{on}}{k_{off}} = \frac{[\text{FixL}-\text{CO}]_\infty}{[\text{FixL}]_\infty[\text{CO}]} \tag{A3}$$

or, at equilibrium

$$k_{on}[\text{FixL}]_\infty[\text{CO}] = k_{off}[\text{FixL}-\text{CO}]_\infty \tag{A4}$$

and in keeping with conservation of mass

$$[\text{FixL}]_\infty + [\text{FixL}-\text{CO}]_\infty = [\text{FixL}] + [\text{FixL}-\text{CO}] \tag{A5}$$

The rate of disappearance of FixL can be expressed as

$$\text{rate} = -\text{d}[\text{FixL}]/\text{d}t = k_{on}[\text{FixL}][\text{CO}] - k_{off}[\text{FixL}-\text{CO}] \tag{A6}$$

rearranging conservation of mass expression:

$$\begin{aligned}[\text{FixL}-\text{CO}] &= [\text{FixL}]_\infty + [\text{FixL-CO}]_\infty - [\text{FixL}] \\ &= K[\text{FixL}]_\infty[\text{CO}] + [\text{FixL}]_\infty - [\text{FixL}] \\ &= (K[\text{CO}] + 1)[\text{FixL}]_\infty - [\text{FixL}] \\ &= k_{off}^{-1}(k_{on}[\text{CO}] + k_{off})[\text{FixL}]_\infty - [\text{FixL}]\end{aligned} \tag{A7}$$

now substitute eq A7 into eq A6

$$\begin{aligned}\text{rate} &= k_{on}[\text{FixL}][\text{CO}] - k_{off}[k_{off}^{-1}(k_{on}[\text{CO}] + k_{off})[\text{FixL}]_\infty - [\text{FixL}]] \\ &= k_{on}[\text{FixL}][\text{CO}] - (k_{on}[\text{CO}] + k_{off})[\text{FixL}]_\infty + k_{off}[\text{FixL}] \\ &= (k_{on}[\text{CO}] + k_{off})[\text{FixL}] - (k_{on}[\text{CO}] + k_{off})[\text{FixL}]_\infty \\ &= (k_{on}[\text{CO}] + k_{off})([\text{FixL}] - [\text{FixL}]_\infty)\end{aligned} \tag{A8}$$

Since $[\text{FixL}]_\infty$ (equilibrium [deoxyFixL]) is very small

$$\text{rate} \approx (k_{on}[\text{CO}] + k_{off})[\text{FixL}] = k_{obs}[\text{FixL}] \tag{A9}$$

where

$$k_{obs} = k_{on}[\text{CO}] + k_{off} \tag{A10}$$

REFERENCES

1. David, M., Daveran, M. L., Batut, J., Dedieu, A., Domergue, O., Gai, J., Hertig, C., Boistard, P., and Kahn, D. (1988) *Cell 54*, 671−683.
2. Monson, E. K., Weinstein, M., Ditta, G. S., and Helinski, D. R. (1992) *Proc. Natl. Acad. Sci. U.S.A. 89*, 4280−4284.
3. Zhulin, I. B., Taylor, B. L., and Dixon, R. (1997) *Trends Biochem. Sci. 22*, 331−333.
4. Gilles-Gonzalez, M. A., Ditta, G. S., and Helinski, D. R. (1991) *Nature 350*, 170−172.
5. Agron, P. G., Ditta, G. S., and Helinski, D. R. (1993) *Proc. Natl. Acad. Sci. U.S.A. 90*, 3506−3510.
6. Gilles-Gonzalez, M. A., Gonzalez, G., and Perutz, M. (1995) *Biochemistry 34*, 232−236.

7. Rodgers, K. R., Lukat-Rodgers, G. S., and Barron, J. A. (1996) *Biochemistry 35*, 9539−9548.
8. Miyatake, H., Manabu, K., Adachi, S., Nakamura, H., Tamura, K., Tanida, H., Tsuchiya, T., Iizuka, T., and Shiro, Y. (1999) *Acta Crystallogr. D55*, 1215−1218.
9. Perutz, M. F., Paoli, M., and Lesk, A. M. (1999) *Chem. Biol. 6*, R291−R297.
10. Gong, W., Hao, B., Mansy, S. S., Gonzalez, G., Gilles-Gonzalez, M. A., and Chan, M. K. (1998) *Proc. Natl. Acad. Sci. U.S.A. 95*, 15177−15182.
11. Rodgers, K. R., Lukat-Rodgers, G. S., and Tang, L. (1999) *J. Am. Chem. Soc. 121*, 11241−11242.
12. Gong, W., Hao, B., and Chan, M. K. (2000) *Biochemistry 39*, 3955−3962.
13. Miyatake, H., Mukai, M., Park, S., Adachi, S., Tamura, K., Nakamura, H., Nakamura, K., Tsuchiya, T., Iizuka, T., and Shiro, Y. (2000) *J. Mol. Biol. 301*, 415−431.
14. Anthamatten, D., and Hennecke, H. (1991) *Mol. Gen. Genet. 225*, 38−48.
15. Mukai, M., Nakamura, K., Makamura, H., Iizuka, T., and Shiro, Y. (2000) *Biochemistry 39*, 13810−13826.
16. Rodgers, K. R., Lukat-Rodgers, G. S., and Tang, L. (2000) *J. Biol. Inorg. Chem. 5*, 642−654.
17. Miyatake, H., Mukai, M., Adachi, S., Nakamura, H., Tamura, K., Iizuka, T., Shiro, Y., Strange, R. W., and Hasnain, S. S. (1999) *J. Biol. Chem. 274*, 23176−23184.
18. Lukat-Rodgers, G. S., and Rodgers, K. R. (1997) *Biochemistry 36*, 4178−4187.
19. Hames, B. D., and Rickwood, D. (1981) *Gel Electrophoresis of Proteins*, p 30, IRL Press, Oxford, U.K.
20. Francis, R. T., Jr., and Becker, R. R. (1984) *Anal. Biochem. 136*, 509−514.
21. Gilles-Gonzalez, M. A., Gonzalez, G., Perutz, M. F., Kiger, L., Marden, M. C., and Poyart, C. (1994) *Biochemistry 33*, 8067−8073.
22. Hofrichter, J., Sommer, J. H., Henry, E. R., and Eaton, W. A. (1983) *Proc. Natl. Acad. Sci. U.S.A. 80*, 2335−2339.
23. Yang, Y., and Inouye, M. (1992) *Proc. Natl. Acad. Sci. U.S.A. 88*, 11057−11061.
24. Ninfa, E. G., Atkinson, M. R., Kamberov, E. S., and Ninfa, A. J. (1992) *J. Bacteriol. 175*, 7024−7032.
25. Wolfe, A. J., and Stewart, R. C. (1993) *Proc. Natl. Acad. Sci. U.S.A. 90*, 1518−1522.
26. Swanson, R. V., Bourret, R. B., and Simon, M. I. (1993) *Mol. Microbiol. 8*, 435−441.
27. Kim, K. K., Yokota, H., and Kim, S. H. (1993) *Nature 400*, 787−792.
28. Milburn, M. V., Prive, G. G., Milligan, D. L., Scott, W. G., Yeh, J., Jancarik, J., Koshland, D. E., Jr., and Kim, S. H. (1991) *Science 254*, 1342−1347.
29. Milligan, D. L., and Koshland, D. E. (1988) *J. Biol. Chem. 263*, 6268−6275.
30. Spiro, P. A., Parkinson, J. S., and Othmer, H. G. (1997) *Proc. Natl. Acad. Sci. U.S.A. 94*, 7263−7268.
31. Levit, M. N., Liu, Y., and Stock, J. B. (1998) *Mol. Microbiol. 30*, 459−466.
32. Bray, D., Levin, M. D., and Morton-Firth, C. J. (1998) *Nature 393*, 85−88.
33. Kaplan, N., and Simon, M. I. (1998) *J. Bacteriol. 170*, 5134−5140.
34. Long, D. G., and Weis, R. M. (1992) *Biochemistry 31*, 9904−9911.
35. Bornhorst, J. A., and Falke, J. J. (2000) *Biochemistry 39*, 9486−9493.
36. Germain, R. N. (1997) *Curr. Biol. 7*, R640−R644.
37. Monson, E. K., Ditta, G. S., and Helinski, D. R. (1995) *J. Biol. Chem. 270*, 5243−5250.

BI011237Q